A Appendix: Extra Results and Illustrations

A.1 Additional Results Regarding Convergence and Sampling

The following result characterizes the geometry of irreplaceably optimal paths as consisting of curves lying on the boundary of an obstacle and straight line segments connecting such curves in free space.

Lemma 13. *Let $\sigma : [0,1] \to \mathbb{R}^d$ be an irreplaceably optimal path. Then for every $s \in [0,1]$ for which $\sigma(s) \in \mathrm{int}(\mathcal{C}_{\mathrm{free}})$ there exist $s_1, s_2 \in [0,1]$ for which $s \in (s_1, s_2)$ and $\sigma(s_1), \sigma(s_2) \in \partial\mathcal{C}_{\mathrm{free}}$, and $\sigma([s_1, s_2]) = [\sigma(s_1), \sigma(s_2)]$.*

Proof. Assume $\sigma(s) \in \mathrm{int}\,\mathcal{C}_{\mathrm{free}}$ for some $s \in [0,1]$. Let

$$s_1 := \inf\left\{t \in [0,1] \,:\, [\sigma(t), \sigma(s)] \subset \mathrm{int}(\mathcal{C}_{\mathrm{free}})\right\}, \text{ and}$$
$$s_2 := \sup\left\{t \in [0,1] \,:\, [\sigma(s), \sigma(t)] \subset \mathrm{int}(\mathcal{C}_{\mathrm{free}})\right\}.$$

Assume, contrary to the claim, that the set $\{\sigma(t) \,:\, t \in [s_1, s_2])\}$ is not a straight line. Then there exists some $p \in (s_1, s_2)$ for which $\sigma(p) \notin [\sigma(s_1), \sigma(s_2)]$. Consequently, there exists some $\varepsilon > 0$ for which $B_\varepsilon([\sigma(s_1), \sigma(s_2)]) \cap B_\varepsilon(\sigma(p)) = \varnothing$. Due to continuity of σ, there exist some $\delta_1, \delta_2 > 0$ for which $B_{\varepsilon/2}(\sigma(t)) \subset B_\varepsilon(\sigma(s_1)$ if $t \in [s_1, s_1 + \delta_1)$ and $B_{\varepsilon/2}(\sigma(t)) \subset B_\varepsilon(\sigma(s_2))$ if $t \in (s_2 - \delta_2, s_2]$. Since the line segment $[\sigma(t_1), \sigma(t_2)]$ connecting any $\sigma(t_i) \in B_\varepsilon(\sigma(s_i))$ with $i = 1, 2$ satisfies $[\sigma(t_1), \sigma(t_2)] \subset B_\varepsilon([\sigma(s_1), \sigma(s_2)])$, it follows that $\mathrm{int}(S_\sigma) \neq \varnothing$, which contradicts the assumption that σ is irreplaceably optimal. ■

Our existing results about convergence have focused on $\mathbb{R}^d$ as those configuration spaces have unique geodesics. Figure 15 illustrates a situation in which non-unique geodesics can cause the shortcutting sequence to not converge.

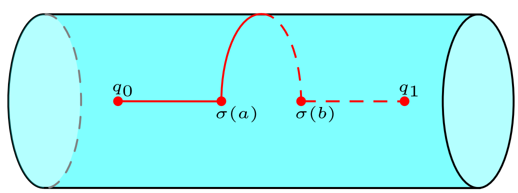

Fig. 15. An initial path on the surface of a cylinder. The path consists of two straight line segments on opposite sides of the cylinder connected by a geodesic. A shortcutting method with a dense sampling sequence will endlessly sample shortcut points with one endpoint on each of the line segments. All such shortcut points have two geodesics, so the sequence of generated paths generated by the shortcut method will not necessarily converge to anything.

For deterministic sequences, our convergence guarantees only apply if the sequence is syndetically dense. The following proposition demonstrates that the Halton sequence is syndetically dense, which provides part of the motivation for its use in our experiments.

Proposition 14 (The Halton sequence is syndetically dense). *The d-dimensional Halton sequence is syndetically dense on* $[0,1]^d$.

Proof. We first argue that the 1-dimensional sequence is syndetically dense on $[0,1]$. Let $p \in \mathbb{N}$, $p > 1$ be the base number corresponding to the Halton sequence, let $(a,b) \subset [0,1]$ and let $k, n \in \mathbb{N}$ be such that $[kp^{-n}, (k+1)p^{-n}] \subset [a,b]$. Write kp^{-n} in base p, so that $kp^{-n} = b_0 p^{-1} + b_1 p^{-2} + \ldots + b_{n-1} p^{-n}$ for some $(b_0, \ldots, b_{n-1}) \in \{0, \ldots, p-1\}^n$. Then the i:th Halton number $r(i,p)$ in the sequence satisfies

$$r(i,p) = a_0(i)p^{-1} + a_1(i)p^{-2} + \cdots + a_m(i)p^{m+1} + \ldots = kp^{-n},$$

if $a_m(i) = b_m$ for all $m \in \{0, n-1\}$ and $a_m(i) = 0$ for $m \geq n$. It follows from the definition of the Halton sequence that every initial segment $\big(a_0(i), \ldots, a_{n-1}(i)\big)$ is repeated cyclically every p^n steps. In addition, the tail $T_n(i,p) := a_n(i)p^{-(n+1)} + a_{n+1}(i)p^{-(n+2)} + \ldots$ contributes to $r(i,p)$ by less than p^{-n}, so that $r(i,p) \in [kp^{-n}, (k+1)p^{-n}] \subset (a,b)$ whenever $\big(a_0(i), \ldots, a_{n-1}(i)\big) = (b_0, \ldots, b_{n-1})$. This proves the claim for $d = 1$.

Assume then that $d > 1$, let $A \subset [0,1]^d$ and let $(p_j)_{j=1}^d$ be the j-tuple of relative primes corresponding to the Halton sequence. Let $C = \operatorname{lcm}\{p_1, \ldots, p_d\}$ be the least common multiple of the base numbers. Then A contains a d-cell of the form $\prod_{j=1}^d [k_j C^{-n}, (k_j+1)C^{-n}]$ for some $k_j \in \{0, 1, \ldots, C^n\}$ and $n \in \mathbb{N}$. It follows from the reasoning above that the i:th term $r(i, p_j)$ of the j:th projected sequence satisfies $r(i,p_j) \in [k_j C^{-n}, (k_j+1)C^{-n}]$ periodically every C^n steps, for every coordinate $j \in \{1, \ldots, d\}$. The claim follows. ■

A.2 Additional Experiments

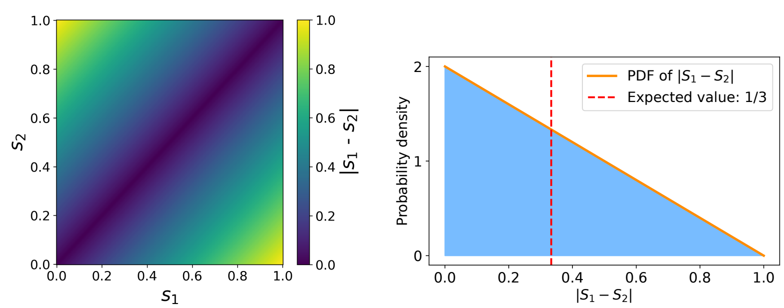

(a) Heatmap (b) Probability density function

Fig. 16. Heatmap of $|s_1 - s_2|$ over $[0,1]^2$ and probability density function of distance Between Two Random Points on $[0,1]$.

Environment 3 In both Figure 17(b) and Figure 18(b), we can see how random and Halton are very close together, although Halton has a slightly lower mean. Slide + Halton does much better than the other methods until around 80 collision checks and from this point on, they all converge very closely. All three methods lower their variability and seem to converge to a cost.

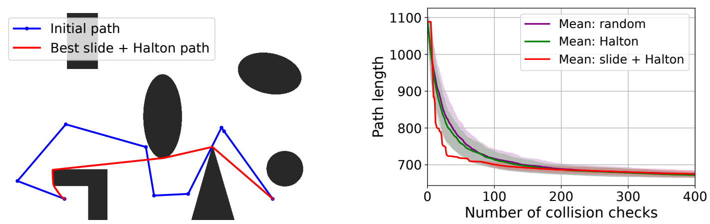

(a) Initial path and converging path for slide + Halton method

(b) For 100 runs of the shortcutting methods, we plot the mean cost with a shaded area representing one standard deviation

Fig. 17. Environment 3, initial path 1, shortcutting methods comparison.

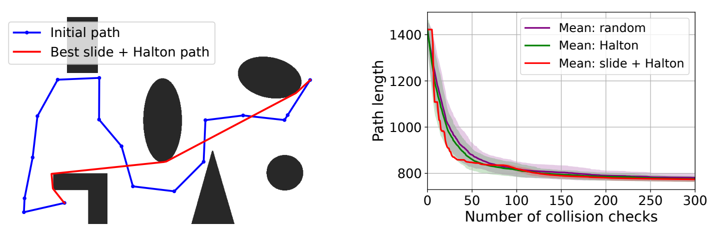

(a) Initial path and converging path for slide + Halton method

(b) For 100 runs of the shortcutting methods, we plot the mean cost with a shaded area representing one standard deviation

Fig. 18. Environment 3, initial path 2, shortcutting methods comparison.

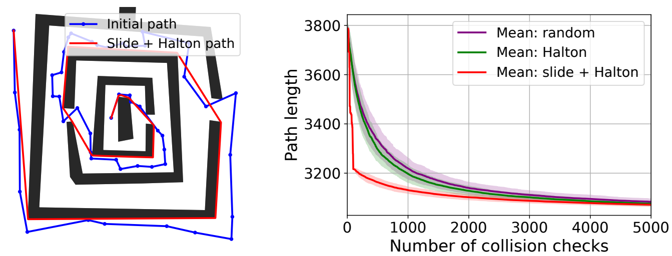

(a) Initial path and converging path for slide + Halton method

(b) For 100 runs of the shortcutting methods, we plot the mean cost with a shaded area representing one standard deviation

Fig. 19. Environment 2, initial path 2, shortcutting methods comparison.

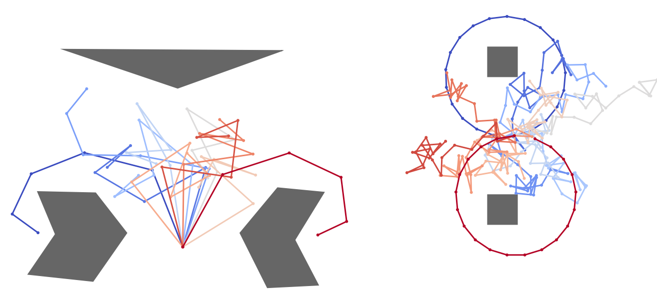

(a)

(b)

Fig. 20. Two different initial paths for multilink arm robots. Each snapshot is a node of the resulting bi-RRT path.

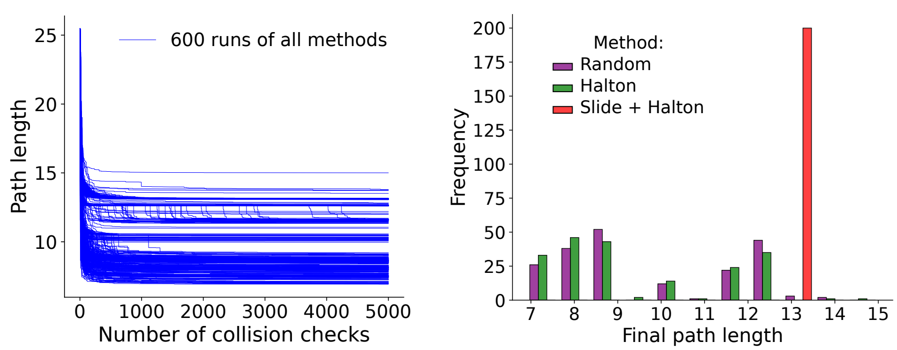

(a)

(b)

Fig. 21. Results of shortcutting methods for the initial path 20(a).

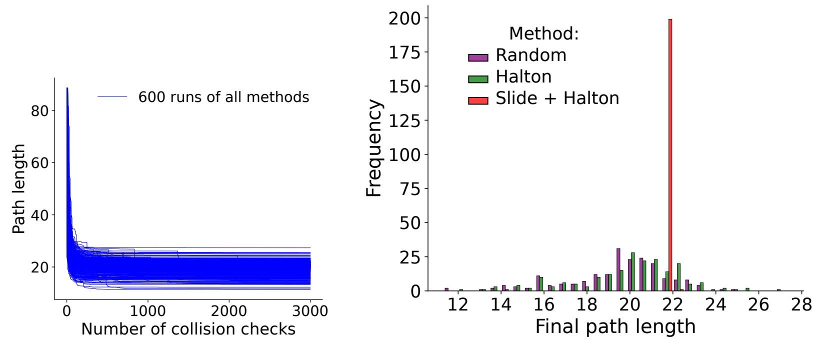

(a) (b)

Fig. 22. Results of shortcutting methods for the initial path 20(b).

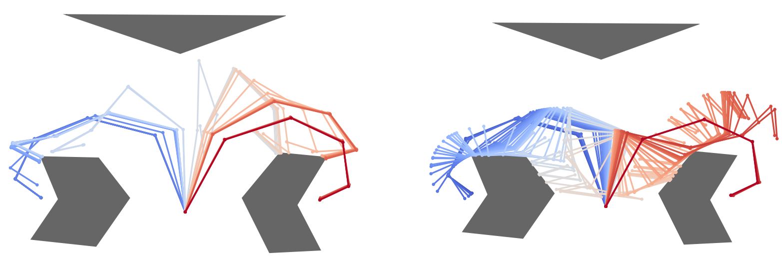

(a) Halton most frequent converging cost: 8.00

(b) Slide + Halton most frequent converging cost: 13.09

Fig. 23. Final paths of shortcutting methods for the initial path 20(a).

(a) Random most frequent converging cost: 19.79

(b) Slide + Halton most frequent converging cost: 21.78

Fig. 24. Final paths of shortcutting methods for the initial path 20(b).